water

MDPI

Article

Effect of Salinity on Evaporation from Water Surface in Bench-Scale Testing

Jared Suchan and Shahid Azam *

Environmental Systems Engineering Faculty of Engineering and Applied Science, University of Regina, 3737 Wascana Parkway, Regina, SK S4S 0A2, Canada; suchan1j@uregina.ca
* Correspondence: shahid.azam@uregina.ca

Abstract: Freshwater and hypersaline lakes in arid and semi-arid environments are crucial from agricultural, industrial, and ecological perspectives. The purpose of this paper was to investigate the effect of salinity on evaporation from water surfaces. The main achievement of this research is the successful capture of simulated climate–surface interactions prevalent in the Canadian Prairies using a custom-built bench-scale atmospheric simulator. Test results indicated that the evaporative flux has a large variation during spring (water/brine: 1452/764 10^{-4} g·s^{-1}·m^{-2} and 613/230 $\times$ 10^{-4} g·s^{-1}·m^{-2} night) and summer (1856/1187 $\times$ 10^{-4} g·s^{-1}·m^{-2} day and 1059/394 $\times$ 10^{-4}g·s^{-1}·m^{-2} night), and small variation in the fall (1591/915 $\times$ 10^{-4} g·s^{-1}·m^{-2} and 1790/1048 $\times$ 10^{-4} g·s^{-1}·m^{-2} night). The primary theoretical contribution of this research is that the evaporation rate from distilled water is twice that of saturated brine. The measured data for water correlated well with mathematical estimates; data scatter was evenly distributed and within one standard deviation of the equality line, whereas the brine data mostly plotted above the equality line. The newly developed 2:1 water–brine correlation for evaporation was found to follow the combination equations with the Monteith model best matching the measurements.

Keywords: evaporative fluxes; distilled water; saturated brine; bench-scale atmospheric simulator

Citation: Suchan, J.; Azam, S. Effect of Salinity on Evaporation from Water Surface in Bench-Scale Testing. *Water* **2021**, *13*, 2067. https://doi.org/10.3390/w13152067

Academic Editor: Svetlozar Velizarov

Received: 14 July 2021
Accepted: 27 July 2021
Published: 29 July 2021

1. Introduction

Freshwater and hypersaline lakes in arid and semi-arid environments are crucial from agricultural and ecological perspectives and for harvesting aquatic food, salt production, and thermal energy [1]. Given that such regions are characterized by a scarcity of surface water, an accurate determination of evaporative flux is paramount to estimate water availability in such facilities. The chemical composition and endorheic drainage (topographical depressions with no apparent outlets) in waterbodies variably affect evaporation [2]. Generally, evaporative flux is governed by several factors such as meteorological parameters, surface temperature, and water salinity [3]. Numerous mathematical formulations have been proposed to estimate freshwater lake evaporation [4]. Although most equations are not adequate to capture the effect of hyper-salinity, some of these can be adjusted by accounting for a reduced saturation vapor pressure [5]. Field studies to validate the accuracy of predictions are affected by complex spatial and temporal variations in atmospheric parameters, water chemistry, and physiographic features [6]. Laboratory experimentation can create a simplified environment by isolating selected influencing parameters provided they are adequately replicated [7].

The Canadian Prairies represent an inland region that experiences minimal precipitation and weather that promotes evaporation from spring to fall [8]. The semi-arid Canadian Prairies has the highest water demand-to-availability ratio in Canada [9] because of low and spatiotemporally variable precipitation [10], a reliance on seasonally variable glacial runoff [11], interprovincial water use agreements [12], and competing municipal and industrial requirements [13]. Evaporation from one of the largest freshwater reservoirs

accounts for more water loss than all other users combined; a 10 mm elevation drop removes 1–4.3 $\times$ 10^6 m^3 of water from the surface [14]. Where freshwater is not available, natural saline lakes often become critical areas for waterfowl and wildlife habitats [15]. Evaporation from saline lakes has negative ecological implications as water loss increases dissolved ion concentration [16]. Furthermore, the potash industry uses freshwater for processing and contains hypersaline residual brine in surface ponds [17]. Evaporation from such storage facilities is critical for mine water recycling [18] and results in a gradually increased level of salt concentration [19].

Figure 1 shows the geographical distribution of freshwater lakes (with less than 0.5 $g{\cdot}L^{-1}$ dissolved salts) and saline lakes (with at least 3.0 $g{\cdot}L^{-1}$ dissolved salts) in Saskatchewan, Canada. Derived from the Wisconsinan Glaciation (2.5 $\times$ 10^6 to 17,000 years B.P.), the terrain is flat and undulating with the last melt of the Laurentide ice sheet (from 17,000 to 8000 years B.P), creating thousands of freshwater lakes with shallow depths and large exposed areas [20]. Likewise, there are approximately 500 saline lakes of at least 1 km^2 areas [1], with high concentrations of dissolved salt [21]. These salts originate from the dissolution of ions as groundwater moved through geologic formations [22]. Alternating carbonate and evaporite formations have led to the development of lean and shallow aquifers (3 $g{\cdot}L^{-1}$ salts comprising Na^+, Ca^{2+}, Mg^{2+}, and $SO_4{}^{2-}$), as well as concentrated and deep aquifers (300 $g{\cdot}L^{-1}$ salts of Na^+ and Cl^-) [2]. Furthermore, several potash tailing ponds exist in the area containing slimes with dissolved salt contents of up to 360 $g{\cdot}L^{-1}$ [19]. In addition, the area is undergoing extensive changes due to the development of an irrigation system with a significant impact on agricultural practices. To ensure sustainable water use in the region (freshwater bodies, saline lakes, and tailings ponds), there is an exigent need to understand the effect of salinity on water evaporation under the prevalent climate.

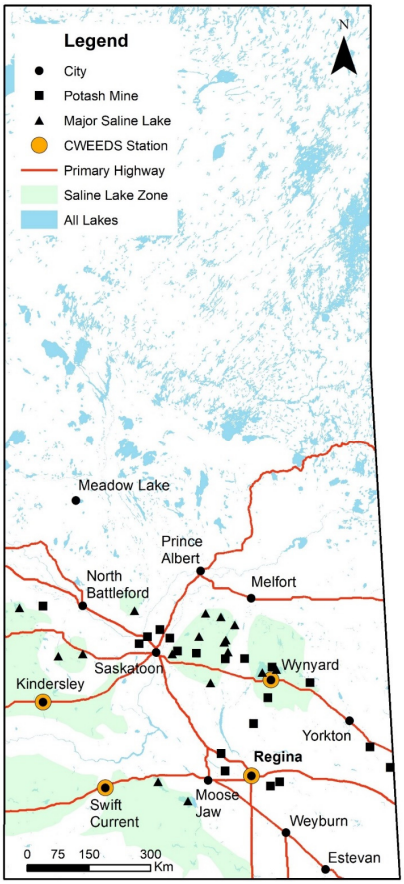

Figure 1. Geographical distribution of freshwater lakes, saline lakes, and potash mines in Saskatchewan, Canada.

The main objective of this research was to investigate the effect of salinity on evaporation using laboratory bench-scale testing. The evaporative fluxes from distilled water and saturated brine were measured under the imposed surface and atmospheric conditions representative of the Canadian Prairies. The two data sets were cross-examined and compared with predictions from established empirical equations.

2. Research Methodology

Evaporative flux tests were conducted using a bench-scale atmosphere simulator developed by Suchan and Azam [23], which replicated six different environmental scenarios in the study area. Table 1 provides the average atmospheric and surface parameters for the selected scenarios (spring, summer, and fall), showing both daytime and nighttime values. Winter was not included because freezing conditions are prevalent during this season. The atmospheric parameters (hourly land-based measurements) were obtained from the Canadian Weather Energy and Engineering Datasets (CWEEDS), based on data from 1998 to 2014. Details on the selection of surface–atmosphere parameters and standard deviations are given in Suchan and Azam [24].

Table 1. Selected atmospheric parameters in the study area, modified after Suchan and Azam [24].

Weather Scenario	Date Range (Month)	Duration (Hours)	Air Velocity ($m \cdot s^{-1}$)	Air Humidity ($g \cdot m^{-3}$)	Air Temperature (°C)	Solar Irradiance ($W \cdot m^{-2}$)	Surface Temperature (°C)
Day	March–November	3706					
Spring	March–May	883	1.7	5.0	10.0	325	12
Summer	May–September	1755	1.3	9.0	19.0	325	22
Fall	September–November	541	1.6	5.0	9.0	210	13
Night	April–November	1827					
Spring	April–May	206	1.3	5.0	9.0	0	6
Summer	May–September	761	1.3	8.5	13.0	0	17
Fall	September–November	277	1.5	5.5	9.0	0	16

The tests were conducted using 15 mL of sample (distilled water and saturated brine) in a clean and air-dried container mounted on an analytical scale balance. The freshwater stock was composed of distilled water containing less than 0.3 $g \cdot L^{-1}$ of dissolved salts. A saturated hypersaline brine stock was prepared by adding 100 mL of distilled water with 35.7 g of NaCl (TDS of 357 $g \cdot L^{-1}$) and stirring until all the solids were completely dissolved. The evaporative flux tests with water were conducted for approximately 3 h similar to İnan and Özgür [25], whereas the brine tests were conducted for approximately 6 h to account for the anticipated reduction in evaporation rate [26]. This generated approximately 1100 measurements for the distilled water and approximately 2200 measurements for the saturated brine at 10 s intervals. The average evaporative flux over the course of each experiment was determined using the change in sample mass over time and the surface area of the sample.

3. Results and Discussion

Table 2 provides a summary of the measured average atmospheric conditions and surface parameters for distilled water and saturated brine tests for the investigated weather scenarios. All of the target weather conditions (air velocity, air pressure, relative humidity, air temperature, and incoming solar irradiance) were achieved. The outgoing shortwave flux was similar between fluids and was found to not exceed 2 W m^{-2} (1% of incoming solar irradiance). This is primarily attributed to the stationary and perpendicular flux source in the atmospheric simulator that does not capture the moving and angular direction of the sun [27] or the effects of latitude [28]. The rate of mass change due to evaporation was obtained from the best fit to measured data (not given in this paper). The resulting values were found to range between 0.9×10^{-4} $g \cdot s^{-1}$ and 2.8×10^{-4} $g \cdot s^{-1}$. Finally, the surface

temperature was achieved for each weather scenario, thereby capturing the long-term heat storage in deep water bodies [29].

Table 2. Summary of the measured average atmospheric and surface parameters.

Parameter	Unit	Symbol	Day						Night					
			Spring		Summer		Fall		Spring		Summer		Fall	
			W	B	W	B	W	B	W	B	W	B	W	B
Count		n	1102	1988	1236	2161	1184	2161	1250	2158	1084	1777	1232	2161
Atmosphere														
Momentum														
Velocity	m·s^{-1}	v	1.7	1.7	1.3	1.3	1.6	1.6	1.3	1.3	1.3	1.3	1.5	1.5
Mass														
Air Pressure	Pa	e_a	94,294	95,893	95,397	95,134	93,414	95,293	94,484	95,845	94,407	93,256	95,060	92,866
Relative Humidity														
Upwind, High	%	h_{UH}	50.8	50.7	51.3	52.0	55.1	53.9	54.4	54.5	75.2	76.0	60.7	64.8
Downwind, High	%	h_{DH}	53.5	53.0	51.9	52.9	57.5	56.4	55.5	55.7	80.5	76.6	61.2	66.1
Upwind, Low	%	h_{UL}	52.7	53.2	55.0	55.3	56.5	56.4	56.6	56.7	75.1	74.9	62.3	62.2
Downwind, Low	%	h_{DL}	55.7	56.2	57.6	57.8	59.9	59.6	59.5	59.5	80.5	80.3	66.2	68.4
Energy														
Temperature														
Upwind, High	°C	T_{aUH}	10.8	11.0	20.7	20.5	9.5	9.8	9.7	9.6	13.7	13.7	9.7	9.4
Downwind, High	°C	T_{aDH}	10.3	10.5	20.4	20.2	9.0	9.3	9.5	9.4	13.0	13.6	9.4	9.1
Upwind, Low	°C	T_{aUL}	10.1	10.1	19.0	19.0	8.9	9.1	9.1	8.9	12.9	13.1	8.9	9.0
Downwind, Low	°C	T_{aDL}	9.9	10.0	19.2	19.1	8.8	9.0	9.0	8.9	13.0	13.1	8.9	9.0
Shortwave Flux (↓)	W·m^{-2}	S_i	325	325	325	325	210	210	0	0	0	0	0	0
Surface														
Mass														
Mass Rate Change ($\times 10^{-4}$)	g·s^{-1}	ΔM	2.17	1.12	2.79	1.72	2.39	1.34	0.93	0.34	1.60	0.59	2.68	1.54
Energy														
Shortwave Flux (↑)	W·m^{-2}	S_o	2	2	2	2	1	2	0	0	0	0	0	0
Temperature	°C	T_s	12	12	22	22	13	13	6	6	17	17	16	16

Note. Surface materials are distilled water (W) and saturated brine (B).

Table 3 gives a summary of the analyzed data of average atmospheric and surface parameters for the investigated weather scenarios. The corresponding transient data (not given in this paper) were found to be steady. The aerodynamic resistance was found to be inversely related to air velocity and ranged from 41 s·m^{-1} to 47 s·m^{-1}. Likewise, the absolute humidity was represented by the lower-upwind hygrometer, and the target results were achieved in the setup. The vapor pressure deficits (atmospheric and surface) were nearly the same for water and brine surfaces because the analyzed values are based on the controlled parameters of humidity, air temperature, and surface temperature. The atmospheric vapor pressure deficit followed the air temperature trends with high diurnal variation in summer (989 Pa and 938 Pa) and negligible variation in spring (83 Pa and 81 Pa) and fall (67 Pa and 69 Pa); values in parentheses are for water and brine, respectively. Similarly, the surface vapor pressure deficit followed the surface temperature trends, with high diurnal variation in summer (685 Pa and 606 Pa) and spring (468 Pa and 438 Pa) and low variation in fall (−256 Pa and −252 Pa).

The determination of energy fluxes was based on an infinitely thin surface with no heat storage [30], such that inputs and outputs were categorized as either radiant, evaporative, sensible, or ground flux, with details provided by Suchan and Azam [24]. The available energy (difference between net radiant flux and ground flux) at the water surface was generally twice that at the brine surface because the presence of salt decreases fluid chemical potential, thereby reducing the latent heat energy of the brines [5]. The diurnal pattern of the available energy was found to be similar to surface vapor pressure deficit, namely: high

variation in the spring (359 $J{\cdot}s^{-1}{\cdot}m^{-2}$ and 194 $J{\cdot}s^{-1}{\cdot}m^{-2}$) and summer (179 $J{\cdot}s^{-1}{\cdot}m^{-2}$ and 195 $J{\cdot}s^{-1}{\cdot}m^{-2}$), and low in the fall (−90 $J{\cdot}s^{-1}{\cdot}m^{-2}$ and −72 $J{\cdot}s^{-1}{\cdot}m^{-2}$); values presented in parentheses are for water and brine, respectively.

Table 3. Summary of the analyzed average atmospheric and surface parameters.

Parameter	Unit	Symbol	Day						Night					
			Spring		Summer		Fall		Spring		Summer		Fall	
			W	B	W	B	W	B	W	B	W	B	W	B
Atmosphere														
Momentum														
Aero. Resistance	$s{\cdot}m^{-1}$	r_a	41.4	41.4	46.6	46.8	42.6	42.6	46.6	46.6	46.6	46.6	43.9	43.9
Mass														
Vapor Density	$g{\cdot}m^{-3}$	ρ_v	5.0	5.0	9.0	9.0	5.0	5.0	5.0	5.0	8.5	8.5	5.5	5.5
Vapor Pressure														
Partial	Pa	e_v	650	658	1209	1215	646	651	652	648	1117	1126	712	715
Saturated	Pa	e_s	1234	1211	2198	2152	1144	1131	1153	1121	1488	1473	1144	1125
Deficit	Pa	e_d	584	554	989	938	498	480	501	473	371	347	431	411
Energy														
Longwave Flux (↓)	$J{\cdot}s^{-1}{\cdot}m^{-2}$	L_i	284	284	340	340	279	280	280	280	313	314	282	283
Surface														
Mass														
Vapor Pressure														
Saturated	Pa	e_f	1402	1375	2646	2593	1498	1468	936	927	1938	1899	1820	1784
Deficit	Pa	e_u	752	717	1437	1379	852	817	284	279	821	773	1108	1069
Energy														
Longwave Flux (↑)	$J{\cdot}s^{-1}{\cdot}m^{-2}$	L_o	367	367	422	422	373	373	337	338	394	394	389	388
Net Radiant Heat Flux	$J{\cdot}s^{-1}{\cdot}m^{-2}$	R	241	241	241	242	117	118	−58	−59	−80	−79	−107	−106
Evaporative Heat Flux	$J{\cdot}s^{-1}{\cdot}m^{-2}$	λE	359	189	464	291	398	226	160	57	258	97	432	258
Sensible Heat Flux	$J{\cdot}s^{-1}{\cdot}m^{-2}$	H	46	24	47	29	112	60	−114	−39	74	28	167	100
Ground Heat Flux	$J{\cdot}s^{-1}{\cdot}m^{-2}$	G	−164	28	−270	−78	−393	−168	−104	−77	−412	−204	−706	−464
Available Energy	$J{\cdot}s^{-1}{\cdot}m^{-2}$	Q	405	213	511	320	509	286	46	19	332	125	599	358
Evaporative Flux ($\times 10^{-4}$)	$J{\cdot}s^{-1}{\cdot}m^{-2}$	ϕ	1452	764	1856	1187	1591	915	613	230	1059	394	1790	1048

Note. Surface materials are distilled water (W) and saturated brine (B).

Evaporative flux was obtained from the measured rate of change in mass and the surface area. The data followed seasonal patterns similar to the surface vapor pressure deficit and the available energy, namely large diurnal variation during spring (839 × 10^{-4} $g{\cdot}s^{-1}{\cdot}m^{-2}$ and 534 × 10^{-4} $g{\cdot}s^{-1}{\cdot}m^{-2}$) and summer (797 × 10^{-4} $g{\cdot}s^{-1}{\cdot}m^{-2}$ and 793 × 10^{-4} $g{\cdot}s^{-1}{\cdot}m^{-2}$), and small variation in the fall (−199 × 10^{-4} $g{\cdot}s^{-1}{\cdot}m^{-2}$ and −133 × 10^{-4} $g{\cdot}s^{-1}{\cdot}m^{-2}$); values presented in parentheses are for water and brine, respectively.

Figure 2 presents the results of the bench-scale testing in the form of evaporation rate with respect to time. As expected, the water loss from distilled water exceeded brine for all of the investigated weather scenarios. The evaporative flux from water surfaces was found to be stable, with data scatter (standard deviation) of 45–64 × 10^{-4} $g{\cdot}s^{-1}{\cdot}m^{-2}$ during the day and 23–27 × 10^{-4} $g{\cdot}s^{-1}{\cdot}m^{-2}$ at night. With the exception of summer day and fall night, a similarly stable flux was observed from brine surfaces with data scatter of 35–45 × 10^{-4} $g{\cdot}s^{-1}{\cdot}m^{-2}$ during the day and 6–57 × 10^{-4} $g{\cdot}s^{-1}{\cdot}m^{-2}$ at night. The evaporative flux gradually increased for brine surfaces during summer day (±162 × 10^{-4} $g{\cdot}s^{-1}{\cdot}m^{-2}$) and fall night (±94 × 10^{-4} $g{\cdot}s^{-1}{\cdot}m^{-2}$) and is attributed to the formation of NaCl crystals. The lower emissivity of solid crystals (ε = 0.87) compared with that of brine fluid (ε = 0.96) interfered with the infrared thermometer, thereby resulting in lower surface temperature readings [31]. These lower readings caused a gradual temperature increase in the silicon heating pad, thereby inadvertently increasing evaporative flux. In each weather scenario, the rate of evaporation from saturated brine surfaces is typically half the distilled water value. In the spring and summer, evaporation is twice as high during the day as compared to night for distilled water and three times higher for brine. Conversely, in the fall scenario,

evaporative fluxes for both water and brine are approximately the same during the day and night.

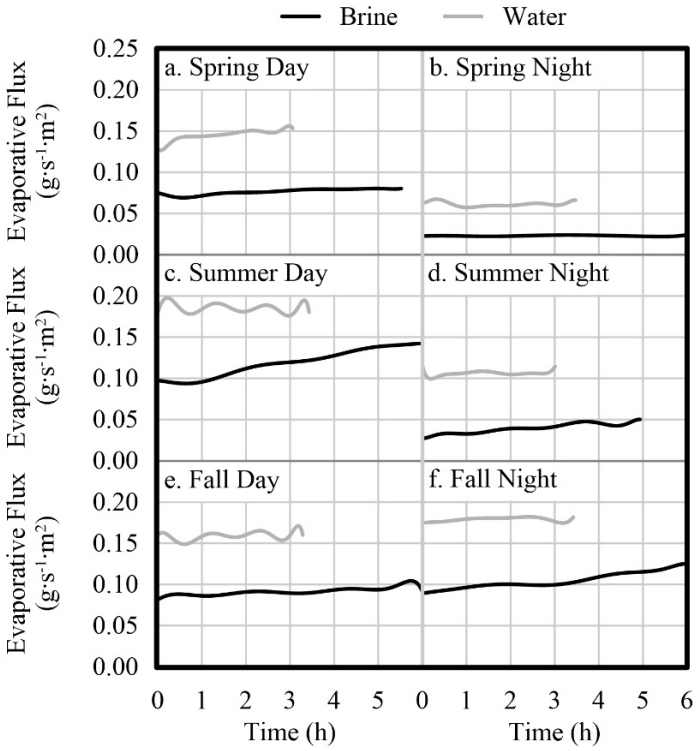

Figure 2. Evaporative flux in the study area for distilled water and saturated brine in (**a**) spring day, (**b**) summer day, (**c**) fall day, (**d**) spring night, (**e**) summer night, and (**f**) fall night.

Figure 3 compares evaporative flux from distilled water and saturated brine surfaces. For the investigated range of surface-atmosphere conditions, the evaporative water flux was more than double that of brine (that is, 2:1 relationship) following a logarithmic equation (R^2 = 0.99). This relationship, along with the associated scatter in data, is primarily related to the effect of NaCl on the measurement of the various parameters during testing.

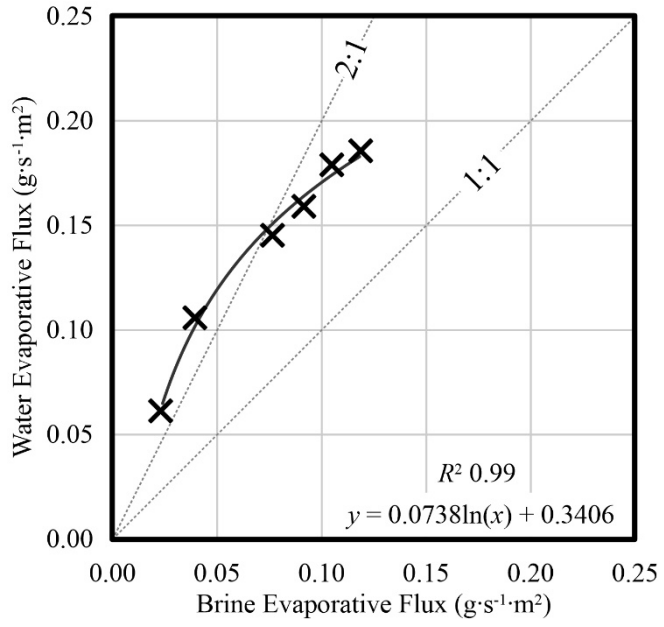

Figure 3. Measured evaporative flux correlation between distilled water and saturated brine surfaces.

Figure 4 compares the measured evaporative flux values with estimates based on empirical relationships relevant to measured data. Table 4 provides a summary of the mass transfer equations such as Himus and Hinchley [32], Meyer [33], and Penman [34] and the combination equations by Monteith [35], De Bruin and Keijman [36], and Duan and Bastiaanssen [37]. The equations are modified to estimate evaporation from saturated brines, under the assumption that dissolved salt reduces the saturation vapor pressure by lowering the activity [5], and can be accommodated in mathematical equations using the concentration of sodium chloride (m) to determine the water activity coefficient [38]:

$$a_w = -0.0011m^2 - 0.0319m \quad (1)$$

For distilled water (Figure 4a), the data are plotted on both sides of the equality line and mostly within one standard deviation of the water data. In contrast, the saturated brine (Figure 4b) is exclusively plotted above the equality line and mostly within one standard deviation of the brine data.

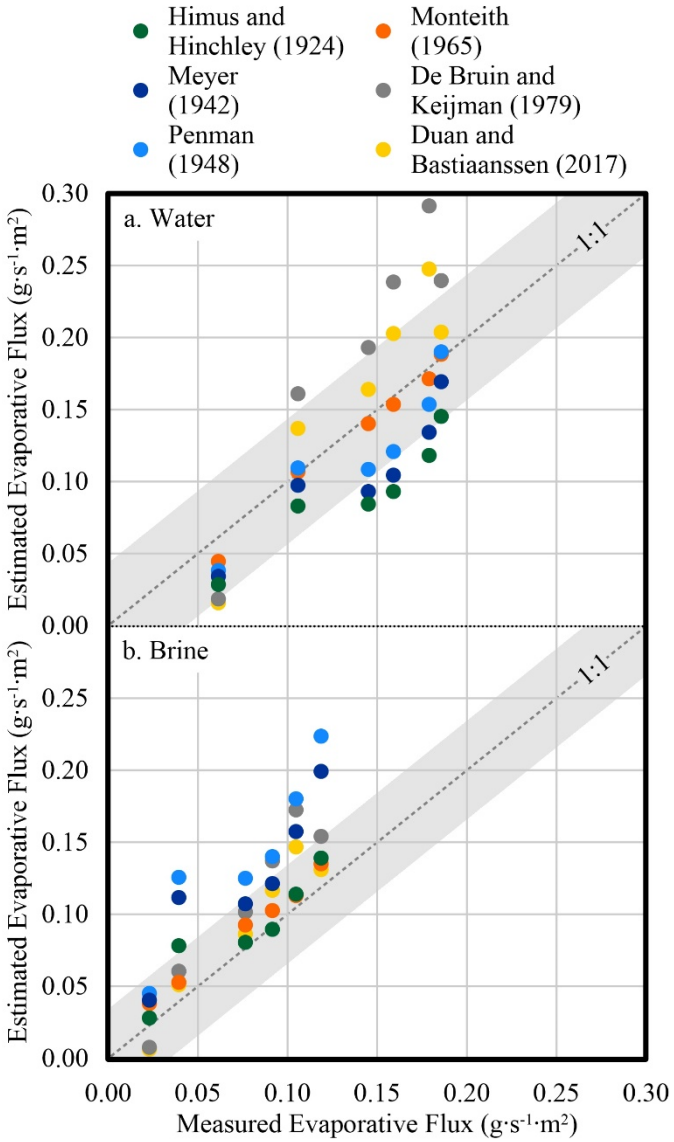

Figure 4. Comparison of estimated and measured evaporative flux for (**a**) distilled water and (**b**) saturated brine.

Table 4. Summary of empirical equations for estimation of evaporative flux, modified after Suchan and Azam [24].

Type and Reference	Vapor Flux Equation ($g \cdot m^{-2} \cdot s^{-1}$)
Mass-Transfer	
[32]	$1 \times 10^{-6}(64.58 + 28.06v)e_d$
[33]	$1.06317 \times 10^{-7}\rho_w(1 + 0.1v)(e_d/1000)$
[34]	$3.3828 \times 10^{-8}\rho_w(1 + 0.24v)(e_d/1000)$
Combination	
[35]	$\frac{1}{\lambda}\left(\frac{\Delta Q + 1.01\rho_a e_u / r_a}{\Delta + \gamma}\right)$
[36]	$\frac{1}{\lambda}\left[\frac{\Delta Q}{(0.85\Delta) + (0.63\gamma)}\right]$
[37]	$\frac{1}{\lambda}\left[\frac{Q - (1.01\rho_a[-0.17T_a + 4.27][1 + 0.536v])}{251}\right]$

Figure 5 and Table 5 compare the estimated evaporative flux values of distilled water and saturated brine for the above-mentioned equations. The mass transfer models were best fitted with linear regressions that remained close to the 1:1 line (R^2 = 0.99 and $TSS = 1 \times 10^{-2}$) because only measured parameters of air velocity and atmospheric vapor pressure deficit are taken into consideration. The trend lines for the Penman and the Meyer equations were found to overlap. All these equations included unique fit parameters that were calculated based on measured data. In contrast, the combination models were best fitted with logarithmic regressions that remained close to the 2:1 line (R^2 ranging from 0.96 to 0.98, and TSS from 1×10^{-2} to 5×10^{-2}), attributed to the inclusion of surface vapor pressure, latent heat, and available energy parameters. These models, which took both mass and energy flux into account, were found to be closer to measured data and captured the logarithmic trend.

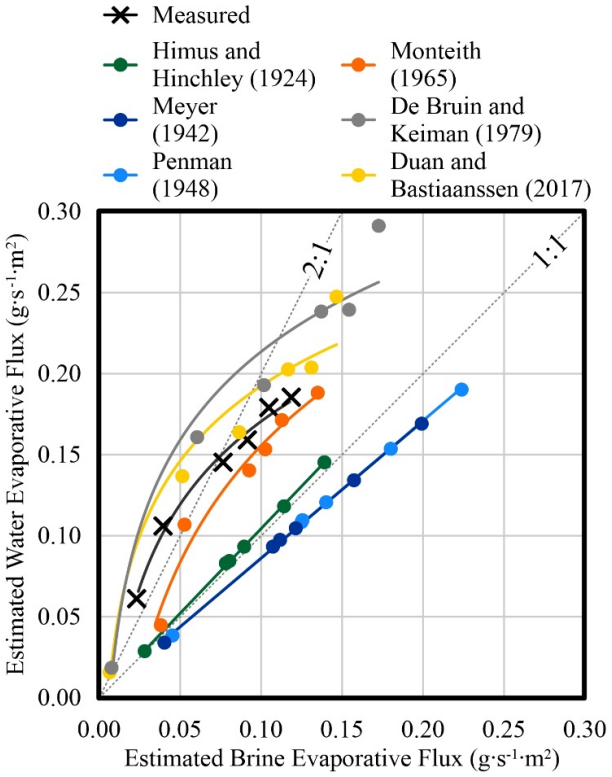

Figure 5. Comparison of evaporative fluxes from distilled water and saturated brine surfaces using various methods.

Table 5. Comparative statistical summary of evaporative fluxes from distilled water and saturated brine surfaces using various methods.

Method	Best Fit	Coefficient of Determination (R^2)	Residual Sum of Squares (SSE)	Regression Sum of Squares (SSR)	Total Sum of Squares (TSS)
BAS2	Logarithmic	0.9910	1×10^{-4}	0.0112	0.0113
[32]	Linear	0.9997	3×10^{-6}	0.0080	0.0080
[33]	Linear	0.9994	6×10^{-6}	0.0102	0.0102
[34]	Linear	0.9997	8×10^{-6}	0.0129	0.0129
[35]	Logarithmic	0.9616	5×10^{-4}	0.0129	0.0134
[36]	Logarithmic	0.9778	2×10^{-3}	0.0433	0.0453
[37]	Logarithmic	0.9559	1×10^{-3}	0.0313	0.0327

4. Summary and Conclusions

A thorough comprehension of evaporative flux from water and brine surfaces in semi-arid climates is necessary to estimate water losses. Laboratory evaporation tests on distilled water and saturated brine were conducted using a custom-built bench-scale atmospheric simulator with climatic parameters and surface conditions representative of the Canadian Prairies. The main conclusions of this study are given as follows:

The test results using a bench-scale atmosphere simulator indicated that the evaporative flux had a large variation during spring (water/brine: $1452/764 \times 10^{-4}$ g·s^{-1}·m^{-2} day and $613/230 \times 10^{-4}$ g·s^{-1}·m^{-2} night) and summer ($1856/1187 \times 10^{-4}$ g·s^{-1}·m^{-2} day and $1059/394 \times 10^{-4}$ g·s^{-1}·m^{-2} night), and small variation in the fall ($1591/915 \times 10^{-4}$ g·s^{-1}·m^{-2} day and $1790/1048 \times 10^{-4}$ g·s^{-1}·m^{-2} night).

The primary theoretical contribution of this research is that the evaporation rate from the distilled water surface is twice that of the saturated brine surface. The measured data for water correlated well with mathematical estimates; data scatter was evenly distributed and within one standard deviation of the equality line, whereas the brine data mostly plotted above the equality line.

The newly developed 2:1 correlation between evaporation rates from water surfaces versus brine surfaces was found to follow the trend lines of the combination equations, and the Monteith model best matched the measure data. In contrast, the mass transfer models were best fitted with linear regressions that remained close to the 1:1 line for water and brine evaporation.

Author Contributions: Data curation and analysis, J.S.; Supervision, S.A.; Writing—original draft, J.S.; Writing—review and editing, S.A. All authors have read and agreed to the published version of the manuscript.

Funding: Natural Science and Engineering Research Council of Canada.

Institutional Review Board Statement: Not applicable.

Informed Consent Statement: Not applicable.

Data Availability Statement: The authors can provide access to test data upon request.

Acknowledgments: The authors would like to thank the University of Regina for providing laboratory space.

Conflicts of Interest: The authors declare there is no conflict of interest.

References

1. Hammer, U.T. Saline lake resources of the Canadian Prairies. *Can. Water Resour. J.* **1986**, *11*, 43–57. [CrossRef]
2. Last, W.M.; Slezak, L.A. The salt lakes of western Canada: A paleolimnological overview. *Hydrobiologia* **1988**, *158*, 301–316. [CrossRef]

3. Salhotra, A.M.; Adams, E.E.; Harleman, D.R.F. Effect of salinity and ionic composition on evaporation: Analysis of Dead Sea evaporation pans. *Water Resour. Res.* **1985**, *21*, 1336–1344. [CrossRef]
4. Finch, J.W.; Calver, A. *Methods for the Quantification of Evaporation from Lakes*; Centre for Ecology & Hydrology: Oxfordshire, UK, 2008.
5. Akridge, D.G. Methods for calculating brine evaporation rates during salt production. *J. Archaeol. Sci.* **2008**, *35*, 1453–1462. [CrossRef]
6. Schulz, S.; Darehshouri, S.; Hassanzadeh, E.; Tajrishy, M.; Schüth, C. Climate change or irrigated agriculture—What drives the water level decline of Lake Urmia. *Sci. Rep.* **2020**, *10*, 236. [CrossRef] [PubMed]
7. Trautz, A.C.; Illangasekare, T.H.; Howington, S. Experimental testing scale considerations for the investigation of bare-soil evaporation dynamics in the presence of sustained above-ground airflow. *Water Resour. Res.* **2018**, *54*, 8963–8982. [CrossRef]
8. Lemmen, D.S.; Vance, R.E.; Campbell, I.A.; David, P.P.; Pennock, D.J.; Sauchyn, D.J.; Wolfe, S.A. *Geomorphic Systems of the Palliser Triangle, Southern Canadian Prairies: Description and Response to Changing Climate*; Natural Resources Canada: Ottawa, ON, Canada, 1998.
9. Faurès, J.M.; Hoogeveen, J.; Winpenny, J.; Steduto, P.; Burke, J. *Coping with Water Scarcity: An Action Framework for Agriculture and Food Security*; Food and Agriculture Organization of the United Nations: Rome, Italy, 2012.
10. Akhter, A.; Azam, S. Flood-drought hazard assessment for a flat clayey deposit in the Canadian Prairies. *J. Environ. Inform. Lett.* **2019**, *1*, 8–19. [CrossRef]
11. Fang, X.; Pomeroy, J.W. Drought impacts on Canadian prairie wetland snow hydrology. *Hydrol. Process.* **2008**, *22*, 2858–2873. [CrossRef]
12. Cutlac, I.; Horbulyk, T.M. Optimal water allocation under short-run water scarcity in the South Saskatchewan River Basin. *J. Water Resour. Plan. Manag.* **2011**, *137*, 92–100. [CrossRef]
13. Wheater, H.; Gober, P. Water security in the Canadian Prairies: Science and management challenges. *Philos. Trans. Math. Phys. Eng. Sci.* **2013**, *371*, 1–21. [CrossRef]
14. Pomeroy, J.W.; Shook, K.R. *Review of Lake Diefenbaker Operations 2010–2011*; Centre for Hydrology, University of Saskatchewan: Saskatoon, SK, Canada, 2012.
15. Hammer, U.T. The saline lakes of Saskatchewan, I. Background and rationale for saline lakes research. *Int. Rev. Gesamten Hydrobiol. Hydrogr.* **1978**, *63*, 173–177. [CrossRef]
16. Bowman, J.S.; Sachs, J.P. Chemical and physical properties of some saline lakes in Alberta and Saskatchewan. *Saline Syst.* **2008**, *4*, 3. [CrossRef] [PubMed]
17. Tallin, J.E.; Pufahl, D.E.; Barbour, S.L. Waste management schemes of potash mines in Saskatchewan. *Can. J. Civil. Eng.* **1990**, *17*, 528–542. [CrossRef]
18. Reid, K.W. Water use in Saskatchewan's potash industry and opportunities for water recycling/conservation. *Can. Water Resour. J.* **1984**, *9*, 21–26. [CrossRef]
19. Landine, P. *Weathering and Diagenesis of Saskatchewan Potash Tailings*; University of Saskatchewan: Saskatoon, SK, Canada, 1993.
20. Christiansen, E.A. The Wisconsinan deglaciation, of southern Saskatchewan and adjacent areas. *Can. J. Earth Sci.* **1979**, *16*, 913–938. [CrossRef]
21. Last, W.M.; Ginn, F.M. Saline systems of the Great Plains of western Canada: An overview of the limnogeology and paleolimnology. *Saline Syst.* **2005**, *1*, 10. [CrossRef]
22. Bredehoeft, J.D.; Blyth, C.R.; White, W.A.; Maxey, G.B. Possible mechanism for concentration of brines in subsurface formations. *Bull. Am. Assoc. Pet. Geol.* **1963**, *47*, 257–269.
23. Suchan, J.; Azam, S. Development of BAS2 for determination of evaporative fluxes. *MethodsX* **2021**, *8*, 101424. [CrossRef]
24. Suchan, J.; Azam, S. Determination of Evaporative Fluxes Using a Bench-Scale Atmosphere Simulator. *Water* **2021**, *13*, 84. [CrossRef]
25. İnan, M.; Özgür, S. Experimental investigation of evaporation from a horizontal free water surface. *Sigma J. Eng. Nat. Sci.* **2017**, *35*, 119–131.
26. Mor, Z.; Assouline, S.; Tanny, J.; Lensky, I.M.; Lensky, N.G. Effect of water surface salinity on evaporation: The case of a diluted buoyant plume over the Dead Sea. *Water Resour. Res.* **2018**, *54*, 1460–1475. [CrossRef]
27. Patel, S.S.; Rix, A.J. The impact of water surface albedo on incident solar insolation of a collector surface. In Proceedings of the 2020 International SAUPEC/RobMech/PRASA Conference, Cape Town, South Africa, 29–31 January 2020; pp. 1–6.
28. Shuttleworth, W.J. Evaporation. In *Handbook of Hydrology*; Maidment, D.R., Ed.; McGraw-Hill Inc.: New York, NY, USA, 1993; pp. 4.1–4.53.
29. Finch, J.W. A comparison between measured and modelled open water evaporation from a reservoir in south-east England. *Hydrol. Process.* **2001**, *15*, 2771–2778. [CrossRef]
30. Granger, R.J.; Gray, D.M. Evaporation from natural nonsaturated surfaces. *J. Hydrol.* **1989**, *111*, 21–29. [CrossRef]
31. Vázquez, O.; Thomachot-Schneider, C.; Mouhoubi, K.; Gommeaux, M.; Fronteau, G.; Barbin, V.; Bodnar, J. Study of NaCl crystallization with passive infrared thermography. In Proceedings of the SWBSS 3rd International Conference on Salt Weathering of Buildings and Stone Sculptures, Brussels, Belgium, 14–16 October 2014.
32. Himus, G.W.; Hinchley, J.W. The effect of a current of air on the rate of evaporation of water below the boiling point. *J. Soc. Chem. Ind.* **1924**, *43*, 840–845. [CrossRef]

33. Meyer, A.F. *Evaporation from Lakes and Reservoirs*; Minnesota Resources Commission: St. Paul, MN, USA, 1942.
34. Penman, H.L. Natural evaporation from open water, bare soil and grass. *Proc. R. Soc. Lond.* **1948**, *193*, 120–145.
35. Monteith, J.L. Evaporation and environment. *Symp. Soc. Exp. Biol.* **1965**, *19*, 205–234. [PubMed]
36. De Bruin, H.; Keijman, J.Q. The Priestley-Taylor evaporation model applied to a large, shallow lake in the Netherlands. *J. Appl. Meteorol.* **1979**, *18*, 898–903. [CrossRef]
37. Duan, Z.; Bastiaanssen, W.G.M. Evaluation of three energy balance-based evaporation models for estimating monthly evaporation for five lakes using derived heat storage changes from a hysteresis model. *Environ. Res. Lett.* **2017**, *12*, 024005. [CrossRef]
38. Lide, D.R. *CRC Handbook of Chemistry and Physics*; CRC Press, Taylor & Francis Group: Boca Raton, FL, USA; London, UK; New York, NY, USA, 2004.